Chapter 2

Microcavities for Silica-Fiber-Based Quantum Information Processing

Hai-Zhi Song

Additional information is available at the end of the chapter

http://dx.doi.org/10.5772/67499

Abstract

High-quality optical microcavities are prospective in many optoelectronics fields like optical communication, nonlinear optics, and quantum information technology. For quantum telecommunication over 1.55 μm silica-fiber-based networks, micropillar cavities containing quantum dots (QDs) are strongly required to construct quantum devices such as single-photon sources (SPSs). The straight way could be using micropillars composed of traditional InGaAsP/InP distributed Bragg reflectors (DBRs), which can in principle serve as efficient 1.55 μm SPSs. To reduce the difficulty in fabricating such ~30 μm high pillars, structure hybridizing semiconductor with dielectric materials is designed. Consisting of Si/SiO_2 DBRs and an InP active layer, such a micropillar readily enhances the rate of single-photon emitting from an InAs/InP QD to be over GHz and serves as a photon-indistinguishable SPS. To strongly couple a 1.55 μm QD with an optical mode, the Si/SiO_2-InP hybrid micropillar cavity can be reformed by introducing tapered DBR structures. This new hybrid pillar cavity can be diminished to have a sub-micrometer diameter, giving small mode volume and ensuring single QD emission. With quality (Q) factor as high as 10^5–10^6, this cavity can behave as a coherently controllable quantum device. More effective might be the InGaAsP/InP-air-aperture micropillar cavity, which can be fabricated by a monolithic process without hybridizing.

Keywords: microcavity, optoelectronics, single-photon source, quantum dot, quantum information processing

1. Introduction

Optical microcavities are widely studied for their prospects in many optoelectronics-related fields of research and technology, such as optical communication, nonlinear optics, and quantum information technology [1–3]. For solid-state quantum information processing, microcavities

containing semiconductor quantum dots (QDs) have been demonstrated to be effective as indispensable devices such as efficient [4–6] and indistinguishable single-photon sources (SPSs) [7] and coherent quantum-control devices [8, 9].

For the purpose of quantum communication over silica-fiber-based networks, InAs/InP QDs are promising as SPSs, as evidenced by their use in quantum key distribution experiments [10, 11]. However, the spontaneous lifetime of InAs/InP QDs is so long (~1.2 ns) that the operation frequency is limited to several hundred MHz. Referred to the key generation rate of attenuated-laser-based QKD systems [12], it is demanding to improve the operation frequency of an InAs/InP quantum dot single-photon source (QD SPS) to the GHz range. For more sophisticated quantum information processing such as quantum repeaters [13], device-independent quantum key distribution [14], and all-optical quantum computing [15], a QD SPS needs to emit highly identical single-photon pulse trains. However, the photon indistinguishability of an InAs/InP QD is still bad due to the big gap between the excitonic coherence time (typically ~100 ps [16]) and the spontaneous lifetime. These two problems can be resolved by introducing InAs/InP QDs into optical microcavities possessing high Purcell factors F_P [6, 7]. Although the emission rate of 1.55 μm InAs/InP QDs was improved by a factor of 5 in a photonic crystal microcavity [17], micropillar cavities are more promising owing to easily isolating single QDs, light emission in the normal direction, and a single-lobed Gaussian-like pattern, which enable high coupling efficiency to fiber [18] and suitability for electrical driving [19]. Here, we are going to study and design micropillar cavities at 1.55 μm telecommunication band for silica-fiber-based quantum information processing.

2. Traditional micropillar cavity

Like the micropillar cavities for InAs/GaAs QDs [5], the straight way to construct an efficient cavity containing InAs/InP QDs might be using a pillar composed of InP-lattice-matched distributed Bragg reflectors (DBRs). On InP substrates, epitaxial growth can produce many types of lattice-matching DBRs including InGaAsP/InP and AlInGaAs/AlInAs. As a representative example, here we will study the former.

As shown in **Figure 1(a)**, the micropillar cavity is a cylinder standing on an InP substrate. It consists of periodic InGaAsP/InP pairs on the top and bottom side of an InGaAsP spacer layer. The InGaAsP/InP periodic structure is the DBRs taking the role of reflecting light toward the spacer. The bottom DBR has more pairs of InGaAsP/InP layers than the top DBRs so that there is less useless leakage to the bottom. Each layer in DBRs is set quarter-wavelength thick, and the spacer layer is one-wavelength thick. The InGaAsP layers are lattice matching to the InP substrate and have an energy gap larger than the photon energy of 1.3 μm wavelength, so that they are extremely transparent for ~1.55 μm light. A light source, representative of an InAs QD, is located in the spacer.

By using finite-difference-time-domain method, the optical properties of this conventional micropillar cavity are simulated. By launching a polarized impulse from the light source, the time evolution of the light intensity can be obtained at monitors set in the spacer layer.

http://dx.doi.org/10.5772/67499

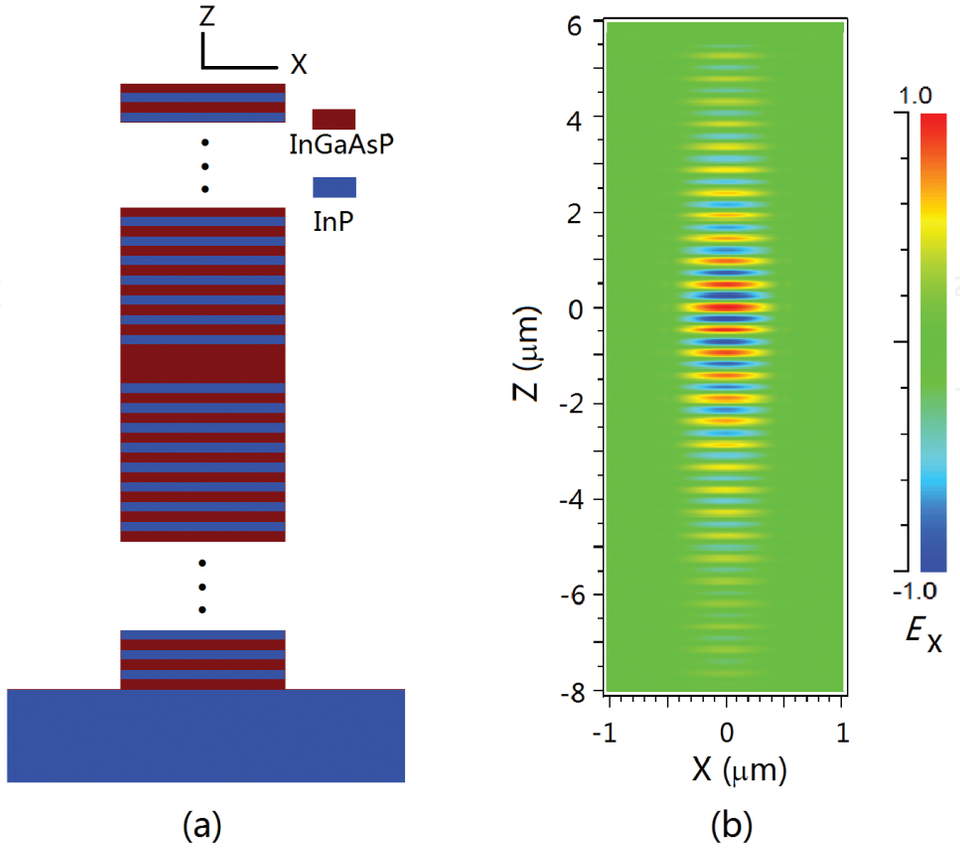

Figure 1. (a) Schematic cross section of the InGaAsP/InP micropillar cavity, (b) distribution profile of the x-polarized electric field E_x of the fundamental mode.

A Fourier transform gives a spectrum of the electric field intensity, showing some peaks representing the cavity modes. By setting the light source as a narrow-band emission around a mode wavelength λ, we obtain the intensity decay with time t and the steady state distribution, i.e., the mode profile. The quality factor Q can be obtained by fitting the exponential light intensity envelope to $\exp(-2\pi ct/Q\lambda)$, where c is the light velocity in vacuum.

The result of this conventional InGaAsP/InP micropillar cavity is as follows. As first, there does exist the fundamental mode peaked near 1.55 μm. The optical field, as shown in **Figure 1(b)**, is confined around the space layer so that the cavity can be of good quality. On a cavity with 30/50 pairs of top/bottom DBR layers, the Q factor is found to be about 2000; 40/70 pairs of DBR layers bring about Q factor close to 10^4. As shown in **Figure 2(a)**, the Q factor looks stable against the change of pillar diameter, which is different from some other micropillar cavities such as GaAs/AlGaAs [5]. It is more meaningful to examine the Purcell factor:

$$F_P = \frac{3Q\lambda^3}{4\pi^2 V n^3}, \tag{1}$$

where λ is the mode wavelength and n is the effective refractive index, and the mode volume:

$$V = \frac{\int \varepsilon(\mathbf{r})\mathbf{E}(\mathbf{r})^2 \mathrm{d}\mathbf{r}}{\varepsilon_M {E_M}^2}, \tag{2}$$

where ε is the relative dielectric constant, **E** the electric field of the light at the position **r**, and ε_M and E_M are the corresponding values at the point of the maximum light intensity. As shown in **Figure 2(b)**, the Purcell factor F_P changes with the cavity size. On a cavity with 30/50 pairs of DBR layers, there often occurs an F_P more than ten. More significantly, a cavity with 40/70 pairs of DBR layers exhibits F_P from 20 to more than 100. This happens with the pillar diameter being less than 1 μm. F_P is small at larger diameters because the mode volume is getting larger.

With the good quality, the above cavity can be considered to be used as a QD SPS. The best single-photon generation rate is inversely proportional to the spontaneous lifetime T_1 of the QD excitons. As such, our cavity with $F_P > 10$ could increase the operation frequency from several hundred MHz into GHz band. For photon indistinguishability, the required F_P is determined by the parameters of the QDs. The main principle is that there should be a coherence time T_2 comparable or longer than $2T_1$. On some InAs/GaAs QDs, remarkable indistinguishability was created by a microcavity with F_P of ~5 [7]. InAs/InP QDs are reported to have T_1 ~ 1.2 ns without a cavity [11] and have T_2 ~ 130 ps [16]. It turns out that a microcavity with $F_P > 2T_1/T_2$ ~ 20 would be required. Obviously, it could be expected that highly indistinguishable single photons could be produced from InAs/InP QDs, using the above traditional InGaAsP/InP DBR-micropillar cavities.

Like the GaAs/AlGaAs micropillar cavities, the InGaAsP/InP one can be in principle fabricated simply by epitaxial growth and dry etching. Noting that such a pillar would be 20–30 μm high, it is actually not easy to fabricate right now. The reason why it needs so many pairs of DBR layers is that InP-lattice-matched material systems such as InP/InGaAsP and AlInGaAs/AlInAs

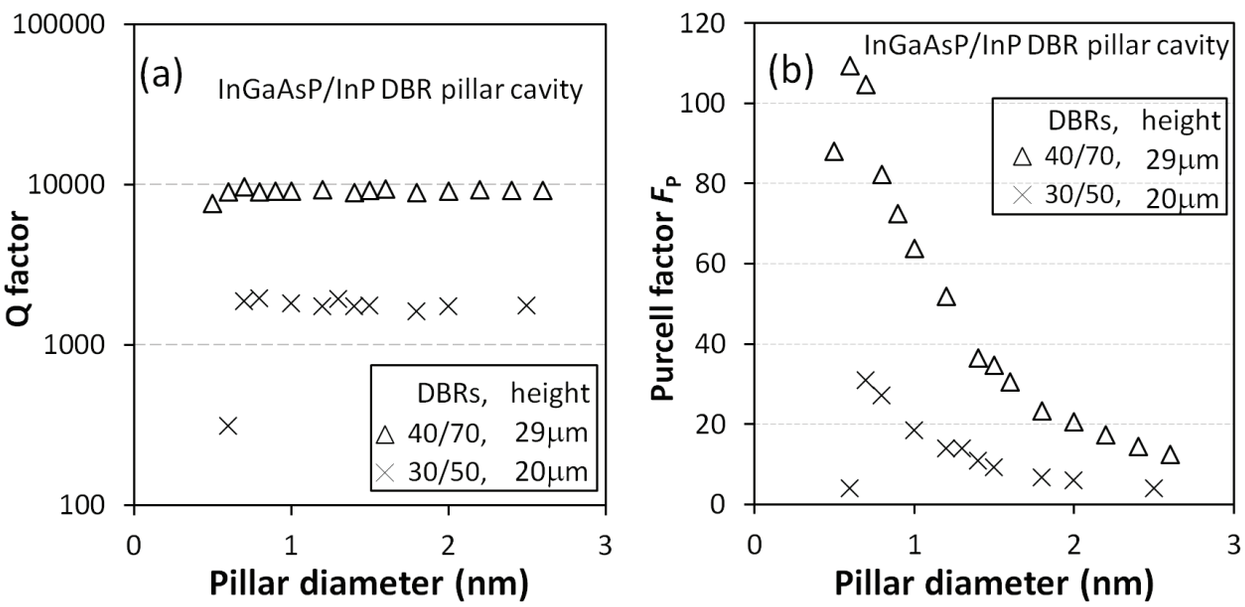

Figure 2. The *Q* factor (a) and Purcell factor (b) as functions of the diameters of InGaAsP/InP micropillar cavities.

http://dx.doi.org/10.5772/67499

have very small refractive index contrast (~0.2) [20]. Nevertheless, since dry-etching process has been available to fabricate pillars higher than 8 μm [21] and epitaxial growth has now enabled layer thickness more than 10 μm, useful InGaAsP/InP micropillar cavities might be producible in the near future.

3. Hybrid micropillar cavity

To resolve the problem with low refractive index contrast in InP-based materials, people may use a hybrid material system. A micropillar cavity consisting of Ta_2O_5/SiO_2 DBRs has been fabricated with an InP spacer containing 1.55 μm InAs/InP QDs [22]. However, this system has not exhibited any Purcell enhancement effect on 1.55 μm QD single-photon emission, because it is still difficult to construct sufficiently many DBR pairs required for enough F_P (noting that the index contrast of ~0.6 is not so large). Si/SiO_2 micropillar cavities have a refractive index contrast as large as ~2, meaning that fewer DBR pairs (than Ta_2O_5/SiO_2) would be sufficient for Purcell enhancement. On the other hand, recent technical advances reveal that wafer bonding [23] and film deposition techniques [24] are ready for hybridizing semiconductor thin layers with Si-based high refractive index contrast multilayers. It is thus relatively easy to fabricate Si/SiO_2 DBR-micropillar cavities with InP spacer layers. Therefore, a micropillar cavity consisting of Si/SiO_2 DBRs and a QD-containing InP central layer is proposed and studied as a Purcell-enhanced single-photon emitter at 1.55 μm [25].

Figure 3(a) shows the vertical xz-plane cross section of the proposed cavity structure. There is an InP layer, which is one-wavelength thick, in the cavity center as the spacer. There are Si/SiO_2 DBRs on the top and bottom sides of the spacer layer. Quarter-wavelength thick SiO_2 and Si layers are alternatively stacking in the DBRs. A light source is settled in the spacer as the InAs/InP QD. Set on a thick Si substrate, the whole micropillar is cylindrically shaped with lateral diameter D on the order of micrometer. With 4/6.5 pairs of the top/bottom DBRs, this micropillar has a pillar height of ~4.5 μm. By calculation using the transfer matrix method, the planar version of this cavity, i.e., with infinite D, is known to have reflectivity of 99.850 and 99.996% at the Bragg wavelength λ_B = 1.55 μm on the top and bottom DBRs, respectively.

The fundamental mode is found significant on this hybrid pillar cavity. At first, its optical field, as shown by the colored pattern in **Figure 3(a)**, is well confined inside the cavity and is highly symmetric. This ensures the usefulness of this cavity as an SPS coupled to fiber. Its mode wavelength λ exhibits a blueshift with respect to the designed Bragg wavelength λ_B = 1.55 μm, as shown in **Figure 3(b)**. As D decreases, the blueshift is getting faster. When $D > 2$ μm, the mode wavelength λ tends to saturate at Bragg wavelength λ_B. This behavior can be explained by waveguide dispersion, as is similar to other micropillar cavities with low index contrasts [26]. In physical sense, it results from more localized geometrical confinement of an optical mode, suggesting shorter mode wavelength, at smaller diameters.

The change of Q factor is somehow similar to the mode wavelength. With decreasing D, its envelope decreases slowly at first and then more rapidly, as shown in **Figure 3(b)**. Mostly larger than a few hundred, the Q factor is likely satisfying an efficient micropillar cavity as a

QD SPS [7]. At the large D extreme, Q factor tends to be close to the value of a planar cavity, ~8000. At the small D extreme, Q degrades to be less than 100. This is attributed to the increased effective incident angle of light on the DBRs [18]. In detail, however, there appear Q oscillations with respect to D, which give relatively high Q in some D areas (e.g., Q = 2000–3300 for D = 2.20–2.40 μm and Q = 3000–4700 for D = 3.20–3.50 μm).

The Purcell factor F_P also exhibits oscillations with respect to D. As shown in **Figure 3(c)**, the F_P oscillations are superimposed on a broad background. This background is mainly attributed to the competition between the opposite effects of Q factor and the mode volume V. It is easy to recognize that the mode volume usually increases with increasing cavity diameter. When D is larger than 1.30 μm, F_P is more than 10 so that the cavity can improve the spontaneous emission rate of a QD by more than one order of magnitude. Corresponding to the high Q areas, there appear also a series of F_P peaks such as F_P = 60–110 at D = 2.20–2.40 μm and F_P = 40–70 at D = 3.20–3.50 μm. By detailed examination, it is known that the maxima of the F_P oscillations are different from that of Q factor. For an example, maximum Q at D = 2.32 μm shifts slightly to D = 2.25 μm for the corresponding F_P maximum.

Further studies should be performed on the Q and F_P oscillations to understand why particular cavity sizes show higher cavity quality. There have reported similar oscillations on low index-contrast DBR-micropillar cavities [27]. These studies suggest that the fundamental HE_{11} cavity mode can be regarded as a combination of a guided HE_{11} mode in the spacer and a Bloch HE_{11} mode in the DBRs. Then, the coupling of these modes with higher-order propagating Bloch modes

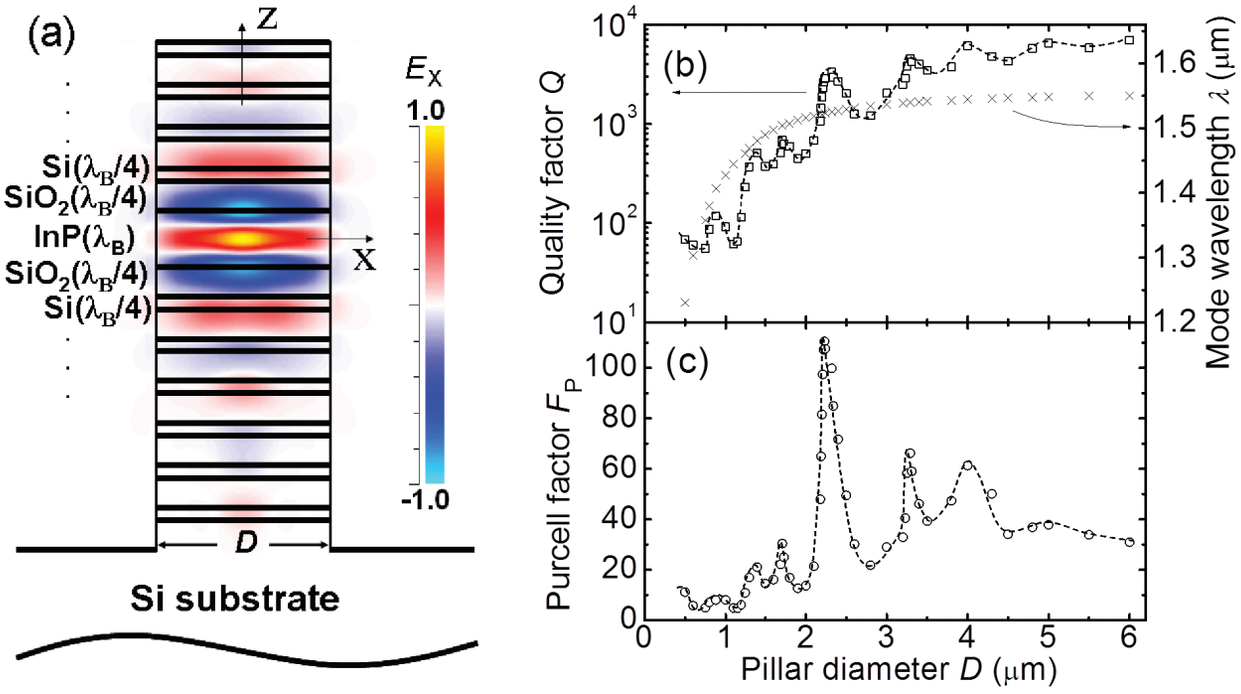

Figure 3. (a) Schematic cross section of the cavity model used for the simulation. The color-scaled pattern shows an example of the x-polarized electric field E_x of the fundamental mode. (b) Mode wavelength λ and quality factor Q and (c) Purcell factor F_P as a function of diameter D for cavities with 4/6.5 top/bottom DBR pairs. The dashed lines are guides for eyes.

http://dx.doi.org/10.5772/67499

gives rise to oscillatory behavior of the Q factor. Shown in **Figure 4(a)** are the x- and y-line profiles and xy-plane profiles of the electric field E_x of the fundamental modes, together with the ideal HE_{11} mode profiles. It is obvious that our cavity shows some fine structures, whereas the standard HE_{11} cavity mode is free of detailed structure. Close to the HE_{11} cavity mode, the profiles at $D = 2.30$ μm exhibit a single lobe at the cavity center and indicate relatively high axial symmetry. However, there remain small shoulders, suggesting a hybrid character of the cavity fundamental mode. Higher-order propagating modes with one or more radial nodes have been incorporated into the fundamental mode. It is worth mentioning that all the mode profiles within $D = 2.20$–2.40 μm are close to $D = 2.30$ μm. Stronger structure details appear in the mode profiles outside this range. It is ring-like at smaller D and has two lobes at larger D. This suggests that different higher-order propagating modes are coupling into the fundamental mode. Similar mode profile variation also happens around some other Q (F_P) peaks such as that at $D = 3.20$–3.50 μm. It is more meaningful to state that, as the result of Q oscillation or mode coupling, a radiation pattern with a single central lobe would be more beneficial for coupling into a fiber.

It is valuable to know how the Q oscillation or the change of mode profiles influences the cavity quality. For this purpose, we can investigate the cavity loss by observing the power flow through the simulation domain surfaces. The cavity loss includes transverse (through sidewalls) and longitudinal (through top and bottom DBRs). The fraction of the longitudinal loss corresponds to Q/Q_{DBR}, where Q_{DBR} is the partial quality factor defined by the loss through the

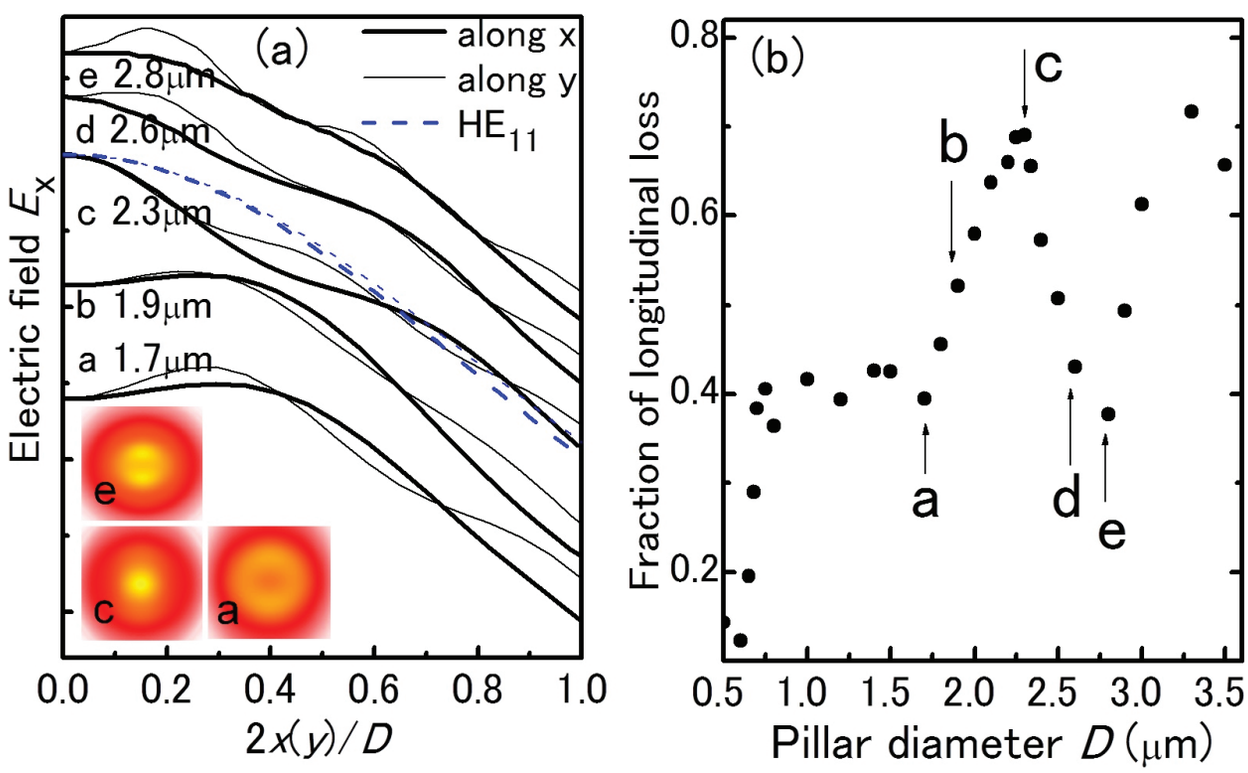

Figure 4. (a) The x- and y-line profiles and the xy-plane profiles (colored insets) of E_x of the fundamental modes in Si/SiO_2-InP hybrid micropillar cavities with different diameters. For clarity, the lines for different sizes are vertically moved away from each other. The blue dashed lines correspond to the ideal HE_{11} mode. (b) The fraction of longitudinal loss, ~Q/Q_{DBR}, as a function of the cavity diameter.

top and bottom DBRs. The fraction of the transverse loss corresponds to $1-Q/Q_{DBR}$. As can be seen in **Figure 4(b)**, Q/Q_{DBR} becomes highest (60–70%) when cavity diameter D is around 2.30 and 3.30 μm. As D deviates from these values, the longitudinal loss decreases. Comparing each mode profile in **Figure 4(a)** with the corresponding loss data in **Figure 4(b)**, one can easily see that a radiation pattern with a single central lobe correlates with the highest fraction of longitudinal loss, which is in practice quite meaningful. The most useful character is the ratio of light output collected in the normal direction. It corresponds to the loss through the top DBR, giving a partial quality factor Q_{top}. Owing to the reflectivity difference between the top and bottom DBR pairs, the loss through the top DBR occupies most, a fraction Q_{DBR}/Q_{top} of ~88%, of the longitudinal loss. The output efficiency can be calculated by $(Q/Q_{DBR})(Q_{DBR}/Q_{top})$ $F_P/(F_P+1)$ [28]. It will thus be ~60% on a cavity with diameter D in the range of 2.20–2.40 or 3.20–3.50 μm, as is an optimized character of the proposed cavity. Noting that the D ranges for high light output (e.g., D ~ 2.30 μm) coincides with those for maximum Q in **Figure 3(b)**, we may argue that a relatively low component of higher-order propagating modes are incorporated into the fundamental mode for single-lobed radiation.

Up to now, we have shown that a 4.5 μm high Si/SiO_2-InP hybrid micropillar cavity with 4/6.5 DBR pairs can present quality good enough for an efficient 1.55 μm band QD SPS. However, the mode wavelength seems not really targeting at 1.55 μm yet. To satisfy a mode wavelength near 1.55 μm, the simplest method may be tuning the Bragg wavelength λ_B to be more than the standard setting λ_{B0}. Setting $\lambda_B = 1.030\lambda_{B0}$, it is found that a cavity with D = 1.30–2.70 μm possesses $F_P > 10$ in the wavelength range of 1.510–1.580 μm. Concrete examples include the following: with D = 1.70 μm, F_P can be ~ 30 at λ =1.550 μm and with D = 2.30 μm, F_P comes up to ~ 100 at λ =1.570 μm. As a practical consideration, it is necessary to further optimize the cavity design for any desired QD emission wavelength. This is actually available if one modifies the design in the high Q (F_P) area, such as D = 2.20–2.40 μm. Viewing λ_B-dependent Purcell factors as a function of D/λ, as shown in **Figure 5(a)**, we learn that they roughly overlaps with that of the λ_{B0} case. It suggests that the best F_P can be obtained for any mode wavelength λ as long as the designs of D and λ_B are suitable. Taking 1.550 μm as the exact target of mode wavelength, we can figure out a cavity design with D = 2.24–2.44 μm and $\lambda_B = 1.017\lambda_{B0}$, resulting in Q = 2000–3300, F_P = 60–110, and λ= 1.550 ± 0.003 μm. For a target wavelength of ~1.580 μm (a practical wavelength for InAs/InP QD SPSs [12]), the best cavity design is determined to be D = 2.28–2.48 μm and $\lambda_B = 1.037\lambda_{B0}$, where Q = 2000–3300, F_P = 60–110, and λ= 1.580 ± 0.003 μm. **Figure 5(b)** displays the typical mode spectra for these two designs. Their line shapes are ideally Lorentzian and their mode widths are less than 1 nm. In addition, good radiation pattern and high output efficiency also remain in these modified designs. However, the spacer thickness was kept wavelength thick (λ_B/n) in all the above designs. The cavity quality could be further improved if the spacer thickness can be freely tuned [29].

It is obvious that our cavity with F_P 10–100 improves the spontaneous emission rate of an InAs/InP QD so that GHz operation of a 1.55 μm QD SPS becomes available. It could also be expected that highly indistinguishable single photons could be produced from InAs/InP QDs, using the above-designed cavities with a nominal F_P = 60–110. In comparison, a Ta_2O_5/SiO_2 cavity of the same quality would need 10/15 top/bottom DBR pairs and a pillar height of 11.5 μm. A practical Ta_2O_5/SiO_2 micropillar cavity, with 8/12 DBR pairs and an 8 μm high pillar

http://dx.doi.org/10.5772/67499

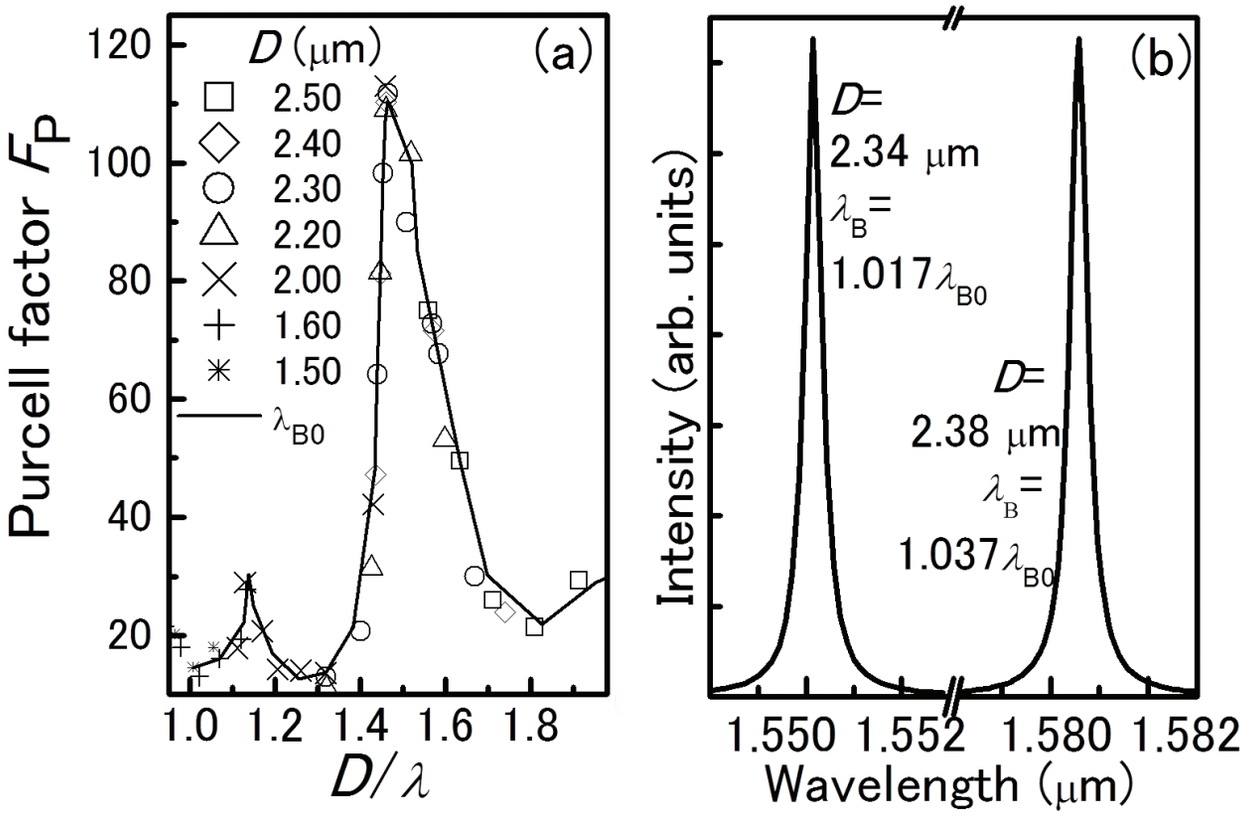

Figure 5. (a) F_P as a function of D/λ in the cases with (symbols) and without (line) tuning λ_B. (b) Two fundamental-mode spectra obtained with chosen diameters D and by suitably tuning λ_B.

[22], would be of lower quality and bulkier than our presently proposed cavities due to a lower refractive index contrast. It is thus reasonable to state that Si/SiO_2-InP hybrid DBR micropillar cavities are better candidates for 1.55 μm InAs/InP QD SPSs.

4. High-quality micropillar cavity

In the above, we proposed a promising micropillar cavity for the 1.55 μm band by combining Si/SiO_2 distributed Bragg reflectors (DBRs) with an InP spacer [25]. This type of microcavity with hybrid materials avoids the difficulty in monolithically fabricating conventional InP-based micropillar cavities. However, this cavity needs relatively large pillar diameter of ~2 μm which is not well satisfying a small mode volume V. This character limits the capability to separate a single QD resonant with the cavity mode and prevents the quantum devices from miniaturizing and integrating. Moreover, future large-scale quantum networks require 1.55 μm SPSs and other quantum devices allowing coherent transfer of quantum states between QDs and single photons via long-distance optical fibers [30], but a Q factor as high as enabling coherent operation seems still difficult in the last hybrid cavity. Very recently, novel structures of micropillar cavities with sub-micrometer diameter and high Q factor were proposed for GaAs/AlAs [31] and TiO_2/SiO_2 [32] systems in which the spacer layers were replaced by tapered DBRs. Although it was proved that such structures were very

effective to obtain improved Q and V, the mode wavelength was shorter than 1 μm. For practical applications, it is required to investigate whether and how the mode wavelength can be extended to 1.55 μm telecommunication band while exhibiting sufficiently high Q factor and small V. Therefore, we present the design of the hybrid micropillar cavity structure consisting of tapered Si/SiO_2 DBRs and InP-based materials containing single InAs QDs [33].

The structure of the proposed micropillar cavity is schematically shown in **Figure 6(a)**. The top and bottom parts of the pillar are conventional DBRs composed of alternating Si and SiO_2 layers. Each layer in these DBRs is set quarter-wavelength thick, i.e., the layer thickness $t_1 = \lambda_B/(4n_{e1})$ for Si, $t_2 = \lambda_B/(4n_{e2})$ for SiO_2, where λ_B is the Bragg wavelength here firstly set to be 1.55 μm and $n_{e1(2)}$ is the effective refractive index of Si(SiO_2), which is calculated and known to be dependent on D by using the standard waveguide theory [34]. In between the conventional DBRs, we incorporate more Si/SiO_2 segments as tapered DBRs on both the top and bottom sides. Here "taper" means adiabatically deducing the layer thicknesses as the DBR extends toward the cavity center (spacer) [31, 32]. In detail, the tapered DBRs have linearly decreasing layer thicknesses $t_{1i} = t_1(1-\rho(2i-1))$ for Si and $t_{2i} = t_2(1-2\rho i)$ for SiO_2, where i is the taper segment number and ρ the tapering slope of the layer thickness, i.e., the decreased fraction per tapered layer. In between the tapered Si/SiO_2 DBRs, an InP layer containing InAs QD as the light source is inserted as the spacer layer with thickness:

$$t_0 = \lambda_B(1 - 2\rho N)/(4n_{e0}), \tag{3}$$

where n_{e0} is the effective refractive index of the spacer material and N the total taper segment number. The whole micropillar is standing on a semi-infinite Si substrate.

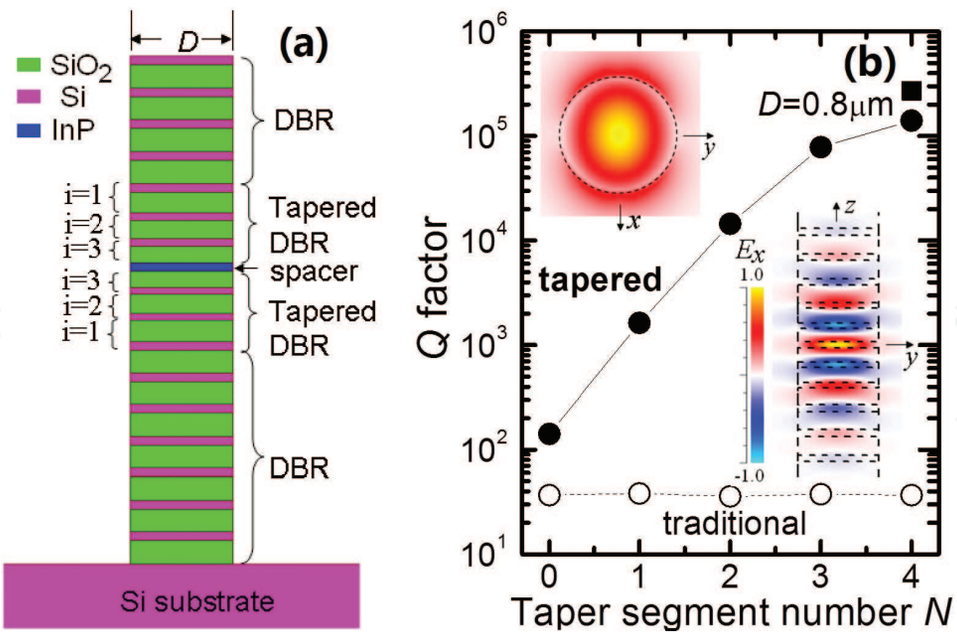

Figure 6. (a) The schematic cross section of the high-quality tapered hybrid micropillar cavity. (b) The Q factors as a function of the total taper segment number for optimized cavities with 0.8 μm of pillar diameter. Those of traditional micropillar cavities are shown as a contrast. Colored insets at the left-up and right-down corners are the profile patterns of E_x of the mainly x-polarized fundamental mode. As a size reference, the cavity outlines are drawn on the mode patterns by dashed lines.

The study was started from all-Si/SiO_2 tapered micropillar cavities, which are similar to the reported tapered cavities absent of a third material [31, 32], by setting the spacer in **Figure 6(a)** to be Si. On such cavities, quality factor Q for the fundamental mode is optimized by simply tuning the tapering slope ρ. Not surprising, a different structure has different ρ for optimizing the Q factor. As an example, a cavity with diameter D = 0.8 μm, DBR of 4/6.5 pairs, and taper segment number N = 3 exhibits an optimized Q factor of 1.1 × 10^5 if ρ = 0.045. Based on the optimized conditions obtained from these all-Si/SiO_2-tapered cavities, one might intuitively expect a good hybrid cavity simply by changing the spacer to InP with the appropriate thickness t_0 determined by Eq. (3), but this does not really give a high Q factor. It is found that it is better to tune the InP spacer thickness as

$$t_0 = \sigma\lambda_B\left(1 - 2\rho N\right)/(4n_{e0}), \tag{4}$$

with the tuning parameter $\sigma > 1$ while using the optimized ρ of the all-Si/SiO_2 case. Naturally, different N corresponds to different σ for the optimized Q factor. Shown in **Figure 6(b)** is the result of an example structure, the cavity with D = 0.8 μm and 4/6.5 pairs of conventional DBRs. It is seen that the Q factor increases monotonically with the total taper segment number N, by in average one order for every additional taper segment.

Compared to traditional counterparts, which have (4+N)/(6.5+N) pairs of quarter-wavelength-thick Si/SiO_2 DBRs and a wavelength-thick InP spacer and show Q factor of below 100, tapered DBRs increase the Q factor for 1–3 orders of magnitude. Typically, the Q factor is increased to be ~ 8 × 10^4 by three segments of tapered Si/SiO_2 DBRs. With 4 taper segments, there seems a saturation effect so that the Q factor reaches 1.4 × 10^5, only about twice that of 3 taper segments. This is because that there are no longer enough conventional DBR pairs to take the role of vertical optical confinement for the would-be higher Q factor. As a matter of fact, when increasing the conventional DBR pairs to 6/9.5, the Q factor can be further increased to be 2.7 × 10^5, as shown by a solid square symbol in **Figure 6(b)**. We may note that the above Q factors are a bit lower than those of all-Si/SiO_2 tapered micropillar cavities. This is the result of replacing Si with InP as the spacer. The mismatch in the refractive indices between Si and InP (~8.5%) determines that the mode-profile matching between the spacer and the DBRs, which is considered to be associated with the Q improvement in tapered cavities [32], is not as perfect as that in all-Si/SiO_2 tapered cavities. Fortunately, the index mismatch is not so large that we can still obtain high Q factors in the Si/SiO_2-InP hybrid tapered micropillar cavities. It can be confirmed by replacing InP with InGaAsP which has an index mismatch of 3.5% with respect to Si. In this case, optimized Q factor of three-segment tapered cavity is ~9.5 × 10^4, much closer to that of all-Si/SiO_2 tapered cavities.

In such a hybrid micropillar cavity, taper design is not necessarily restricted to Si/SiO_2, but we learned that InP/InGaAsP tapered DBRs are far less effective than Si/SiO_2 in improving the cavity quality, because of the difficulty in mode-profile matching between InP/InGaAsP and Si/SiO_2.

The above high Q factors suggest thus the nice property of the presently proposed micropillar cavities. Their good character also lies at the mode profiles, as shown by the insets of **Figure 6(b)**. The mode profile of the fundamental mode is single lobed and highly symmetrical (by the

in-plane xy profile), which makes it beneficial to couple the QD emission from the cavity into a fiber. The mode profile is well confined in the tapered region (by the vertical yz profile), which could probably be one of the reasons for high Q factors in such tapered micropillar cavities.

In optimizing the Q factor by only tuning the parameter σ as in the above, the mode wavelength may not exactly match a specific target wavelength. We can resolve it by tuning the cavity structure together in parameter σ, tapering slope ρ, and Bragg wavelength λ_B, all of which describe the vertical structure of the cavities. For the last parameter λ_B, we label the previous setting as λ_{B0} = 1.55 μm from now on. Using these procedures on three-segment tapered cavities with D = 0.8 μm and 4/6.5 conventional DBR pairs, we find that the best Q factor of 8×10^4 for an exact mode wavelength λ = 1.550 μm can be obtained by setting σ = 1.18, ρ = 0.05, and $\lambda_B = 1.02\lambda_{B0}$.

An optimized design needs detailed knowledge of the dependence on various parameters, which is a little complicated. For simplification, we here characterize the effects of the three tuning parameters σ, ρ, and λ_B in terms of the variation in spacer thickness $\Delta t_0 = t_0 - t_{0m}$, since they all give rise to changes in the spacer thickness t_0. **Figure 7(a)** shows the mode wavelength and the Q factor depending on $\Delta t_0/t_{0m}$, the relative change in the spacer thickness, in the three cases of cavity structure tuning. As σ only is tuned, meaning that only the InP spacer thickness is changing, the mode wavelength changes weakly, but the Q factor degrades fast. Viewed in a wider range, the variation of Q factor is actually something like a degrading sinusoidal function of the spacer thickness (not shown). As the spacer thickness increases, it is deduced to a minimum of ~100 at $\Delta t_0/t_{0m}$ ~ 1.1, then comes up again to another maximum of ~ 500 at $\Delta t_0/t_{0m}$ ~ 2.5, and goes down once more. As the tapering slope ρ only is tuned, meaning that the tapered DBRs and the spacer are changing together, the mode wavelength changes faster, but the Q factor decreases more slowly. As the Bragg wavelength λ_B only is tuned, meaning that the thicknesses of all layers are changing, the mode wavelength changes even faster, but the Q factor almost remains high. As a whole, Q factor can be preserved over 10^4, while the mode wavelength λ is limited within the range of 1.50–1.60 μm, if the layer thickness fluctuation is within ±5%, as is indicated by a shaded area in **Figure 7(a)**.

The above Q variations versus vertical structure suggest that a local change destroys, while an overall harmonic change keeps the quality of a cavity. To further understand it, we may try viewing the mode-profile matching, which was considered responsible for high Q factors in tapered cavities [32]. **Figure 7(b)** shows the line profiles of the fundamental mode along the in-plane y direction for a few cavity structures O, A, B, and C, as marked in **Figure 7(a)**. The two lines in each set are taken from the central planes of the spacer layer and of the Si layer closest to the spacer. It is clear that the optimized cavity structure O shows good mode matching. The structure A, whose Q factor is just a bit lower than structure O, has mode matching a little bit worse than structure O. The structure B, whose Q factor is greatly degraded, has remarkably mismatching mode profiles. However, the structure C has mode matching not as bad as structure B but as good as structure A although its Q factor is even worse than structure B. It suggests that mode-profile mismatching only cannot perfectly explain the Q factors of our tapered micropillar cavities. Probably, phase mismatching [35] may take a role in determining the Q factor, which is open for future investigation.

http://dx.doi.org/10.5772/67499

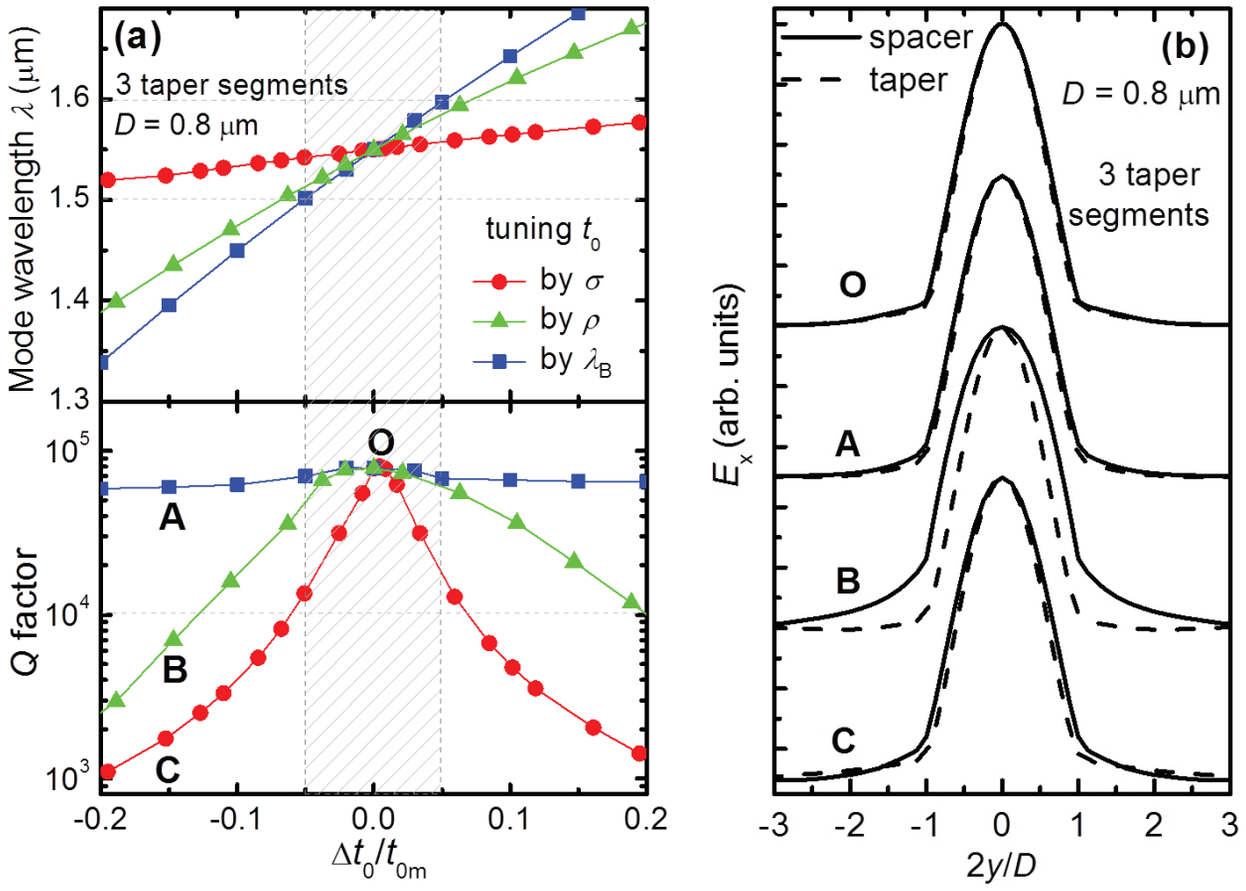

Figure 7. (a) Mode wavelength λ and Q factor as functions of the relative variation in the spacer thickness in different parameter-tuning cases for typical tapered hybrid micropillar cavities. (b) Line profiles of the electric field E_x of the fundamental modes in the central plane of the spacer (solid) and of the Si layer closest to the spacer (dashed) for four different cavity structures as marked in (a). For clarity, the lines for different cavity structures are vertically shifted away from each other.

After describing the dependence on the vertical structure as above, we examine here how the cavity property varies with the lateral size, the pillar diameter D. As examples, we show the results of three structures as depicted in **Figure 8**.

The red square symbols in **Figure 8(a)** and **(b)** show that, with 2/3.5 pairs of conventional DBRs and two tapered segments, an optimized Q factor of more than 3000 for 1.55 μm emission happens with pillar diameter of 0.85 μm, and changing the pillar diameter in 0.60–0.95 μm gives Q factors of over 1000 for wavelength 1.35–1.60 μm. Compared to the last hybrid cavity, the Q factor is the same, and the Purcell factor F_P, shown in **Figure 8(c)**, is somehow higher because the pillar diameter is greatly decreased to below 1 μm. Besides, the pillar height remains the same as the last one, 4.5 μm, suggesting the superiority of this cavity beyond the previous structure in generating indistinguishable single photons and enabling ultrahigh-speed SPSs operating in several GHz clock.

The more typical is the structure with 4/6.5 pairs of conventional DBRs and three taper segments, whose vertical structure is fixed to that optimized with D = 0.8 μm. The blue circles in **Figure 8** show that the Q factor of this structure is 1–8 × 10^4 in the range of D = 0.45–1.10 μm, 1–2 orders

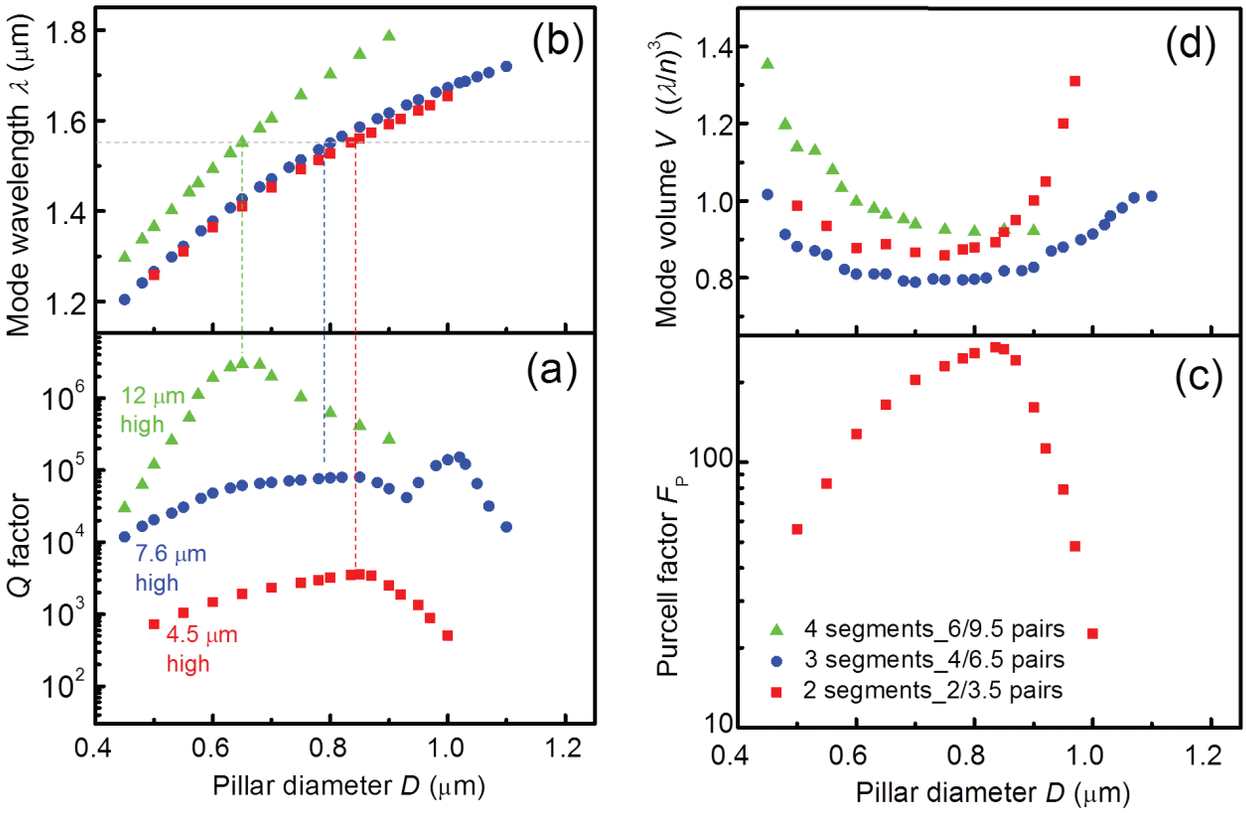

Figure 8. The (a) Q factor, (b) mode wavelength λ, (c) Purcell factor F_P, and (d) mode volume V as functions of the pillar diameter D for the tapered Si/SiO_2-InP micropillar cavities with vertical structures fixed at optimized conditions.

of magnitude higher than that of the previous cavities, from below 100 for $D < 1$ μm to a few thousands for $D > 2$ μm. Especially, it remains over 6×10^4 in a D range of 0.65–0.90 μm, exhibiting the robustness against diameter variation. There is a peak around $D = 1.0$ μm, appearing somehow abnormal. It is probably a result of oscillation behavior also observed in GaAs/AlAs tapered cavity [31] and is probably related to the coupling with higher-order modes, which often occurs in the previous micropillar cavities [36]. This good quality is in debt to a ~7.6 μm high micropillar, higher than that of the last hybrid cavity, because not only of tapered layers incorporated but also of smaller effective refractive indices, increasing the thickness of each DBR layer.

Similarly, we examined cavities with 6/9.5 conventional DBR pairs and four taper segments. We fix the vertical structure to an optimized cavity with $D = 0.65$ μm, which gives a Q factor as high as 3×10^6 at mode wavelength of 1.55 μm. Fixing the vertical structure to this condition, we get the cavity properties as functions of the pillar diameter D, as shown in **Figure 8** by green triangle symbols. At the expense of a pillar height 12 μm, a Q factor of over 1×10^5 can be obtained in a cavity with diameter ranging from 0.5 to 0.9 μm. Especially, $Q > 2 \times 10^6$ are available for mode wavelength $\lambda = 1.55 \pm 0.05$ μm with $D = 0.60$–0.70 μm in this cavity. Since the traditional cavities with 6/9.5 DBR pairs have typically just ~20% higher Q factors (not shown) than 4/6.5 DBR pairs, the four-segment tapered cavity here improves the Q factor for 2–3 orders of magnitude.

Just due to thicker DBR layers, all these three structures show mode wavelength varying with the diameter D faster than that of the previous cavities, as seen in **Figure 8(b)**. **Figure 8(c)** does not show F_P for three and four taper segments because most of their nominal values are too high to be physically meaningful due to the property beyond weak coupling regime. As another important parameter, the mode volume V of these cavities is shown in **Figure 8(d)** in the unit of $(\lambda/n)^3$, where n is the refractive index of the spacer material. It is found mostly less than 1, which is not so different but definitely smaller than that of the previous cavity in the small D area, although recent study suggests significant reduction of the mode volume as low as ~0.1 with the benefit of the tapered DBRs [32]. Anyway, the structure with three taper segments can typically have V as small as ~0.8, which is reduced to be half of that of our last hybrid cavities, ~1.6 at D ~ 2.2 μm.

In the above, the allowed pillar diameter for mode wavelength around 1.55 μm is restricted to a small range spanning within 0.1 μm, due to fixed vertical structures. This, however, does not mean that an effective cavity for ~1.55 μm band can only be obtained in such a narrow size range. By employing vertical structure tuning at various diameters, we can see that a high Q factor for mode wavelength of ~1.55 μm is available in a wider diameter range. Q factors over 6×10^4 can be obtained with pillar diameter of 0.70–0.95 μm. The degradation of Q factor at diameter less than 0.6 μm is partly because that lateral confinement of the optical mode is more difficult. There is a peak at D = 0.9 μm, appearing somehow unusual though good for application. Similar to the case of fixed vertical structure, this is probably a result of oscillation behavior likely related to the coupling with higher-order modes. Generally, based on vertical cavity structures of high Q factors, tapered Si/SiO_2-InP micropillar cavities with sub-micrometer diameters can have Q factors of near 10^5 to a few 10^6, improved for up to three orders of magnitude compared to the previous ones, with mode wavelength of 1.55 ± 0.05 μm.

With the good properties described above, we shall now discuss our tapered Si/SiO_2-InP micropillar cavities on their effectiveness for applications.

At first, for SPS-based quantum devices, it is important to isolate a single QD effectively emitting from the cavity. Supposing a high QD density of the order of 10^{10} cm^{-2} and an inhomogeneous width of ~50 meV, there could be less than 1 QD resonant to a cavity mode with Q factor more than 3000 in a cavity with diameter of 1 μm. It guarantees the single-photon nature of an InAs/InP QD SPS using this sub-micrometer micropillar cavity. Since the saturated effective emission rate is proportional to the square of the coupling strength $g^2 \propto 1/V$ [37], the small mode volume helps increasing the limit in the quantum key rate of an SPS by a factor of 2 with respect to the previous case. This is quite beneficial to enable ultrahigh-speed SPSs operating in several GHz clock.

Coherent operation of SPS requires strong coupling between the QD and the cavity mode, which can be satisfied if [37]

$$g/|\kappa - \gamma - \gamma * | > 1/4 \tag{5}$$

where g is the coupling strength, $\kappa = 2\pi c/Q\lambda$ the loss rate of the cavity mode, γ the spontaneous emission rate, and γ^* the pure dephasing rate of the QD. When Q is not higher than a few 10^4, κ is much larger than $\gamma = 1/T_1$ (T_1 ~ 1.2 ns [12]) and $\gamma^* = 1/T_2^* = 1/T_2 - 1/2T_1$ (T_2 ~ 0.13 ns

[17]) [38], so the condition in Eq. (5) can be simplified as $g > \kappa/4$. Using $g = \sqrt{e^2 f/(4\varepsilon_0 n^2 m_0 V)}$ [31], where ε_0 is the vacuum permittivity, e the elementary charge, m_0 the free-electron mass, and $f = \varepsilon_0 m_0 c\lambda^2/(2\pi n e^2 T_1)$ [39] the oscillator strength of the QD; the simplified condition reads $Q/\sqrt{V} > \sqrt{\pi\lambda/r_e nf}/2 = 2200$, where $r_e = e^2/(4\pi\varepsilon_0 m_0 c^2)$ is the classical radius of electron and V is the mode volume normalized to $(\lambda/n)^3$. As Q goes higher than that of the satisfied simplified condition, Eq. (5) is always available since $|\kappa - \gamma - \gamma^*|$ is decreasing to zero and then approaching $\gamma + \gamma^*$ (~30 μeV), which is much less than $4g$ (~365 μeV). Obviously, this condition can be easily satisfied by our tapered micropillar cavity since its $Q/\sqrt{V}$ can be ~10^5–10^6 and ~2–3 orders of magnitude higher than that of the previous cavity, maximally ~ 2000. It is indicative of the feasibility of constructing a coherent SPS or other quantum devices for 1.55 μm band quantum information processing.

As the actual fabrication process is concerned, our cavity design has an advantage in lowering the pillar height as compared with those of GaAs/AlAs and SiO_2/TiO_2 tapered micropillar cavities. The GaAs/AlAs case gives a pillar height of 9.6 μm for mode wavelength λ ~ 0.9 μm [31]; then it would be ~16 μm high for λ ~1.55 μm. The TiO_2/SiO_2 tapered cavity gives a pillar height of 6.2 μm for λ ~ 0.64 μm [32]; thus it would be ~15 μm high for λ ~ 1.55 μm. Our present cavities thus serve as better candidates for λ ~ 1.55 μm.

Finally we may argue that the tapered Si/SiO_2-InP hybrid micropillar cavities here proposed are not only promising as 1.55 μm quantum information processing devices based on InAs/InP QDs; their high Q and small V also support the applications in other fields such as ultrasmall lasers, slow-light engineering, and optical switching.

5. High-quality and monolithic microcavity

Although being of high quality at 1.55 μm telecommunication band, the hybrid tapered Si/SiO_2-InP hybrid micropillar cavity is not yet ideal due to the complicated fabrication process, defecting near the light source caused by thin active layer and mismatching thermal expansion in different materials. As a matter of fact, up to now a practically good pillar cavity has not been available yet as a SPS applied in 1.55 μm quantum information processing. More efforts must thus be devoted to finding methods of overcoming the left problems. We are herewith considering some techniques beyond material hybrid. In the case of planar DBR cavity, an effective way to increase refractive index contrast of InP-based materials is to introduce air gaps by sacrificing some layers [20, 40]. We note that a pillar DBR cavity might be reformed by incorporating partial air-gap layers. In this section, therefore, we propose a micropillar cavity consisting of InGaAsP/InP layers with partial air gaps, which can be monolithically fabricated. It is presented that this microcavity has high quality (Q) factors and small mode volumes, satisfying the requirements of SPS at 1.55 μm telecommunication band.

The proposed cavity structure is schematically demonstrated in **Figure 9(a)**. It shows that disk-shaped (in the XY plane) and coaxially set (in the Z direction) InGaAsP and InP layers with different diameters D and d, respectively, are alternatively stacked on an InP substrate. Effectively, the small-sized InP layers are compassed by surrounding air gaps, or, namely, with air

http://dx.doi.org/10.5772/67499

apertures. The InGaAsP layers are lattice matching to the InP substrate and have an energy gap larger than the photon energy of 1.3 μm wavelength, so that they are extremely transparent for ~1.55 μm light.

In more detail, the top and bottom parts of the cavity are conventional DBRs composed of periodical InGaAsP and InP layers. Each InP layer in the DBRs is set as thick as $t_1 = \lambda_B/4$, where λ_B is the Bragg wavelength, set to be around 1.55 μm. This thickness is actually a quarter-wavelength of air because the optical media of this layer in the pillar is mainly air rather than InP. In the case of planar air-gap DBR cavities [20, 40], semiconductor layers are usually set to be three-quarter-wavelength thick, but our simulation implies that this design in our case hardly has good cavity quality. Thus the InGaAsP layers in the DBRs are set quarter-wavelength thick, i.e., $t_2 = \lambda_B/(4n_2)$, where n_2 is the refractive index of InGaAsP. Inserted between the conventional DBRs are more InGaAsP/InP-air-aperture segments (pairs) as tapered DBRs on both the top and bottom sides. In detail, the tapered DBRs have linearly decreasing layer thicknesses $t_{1i} = t_1(1-\rho(2i-1))$ for InP and $t_{2i} = t_2(1-2\rho i)$ for InGaAsP, where i stands for the taper segment number and ρ is the tapering slope of layer thickness, i.e., the decreased fraction per tapered layer. In between the tapered DBRs, an InP layer is inserted as the spacer layer with thickness $t_0 = t_1(1-2\rho N)$, where N is the total taper segment number in one tapered DBR. An InAs QD is set in this layer as the light source.

It is found that the InGaAsP/InP-air-aperture microcavity is of high quality when it has 4/6.5 pairs of InGaAsP and InP layers in the top/bottom DBRs and $N = 3$ segments in the tapered DBRs. The pillar of this cavity structure appears some 7–8 μm high, which is the same as the

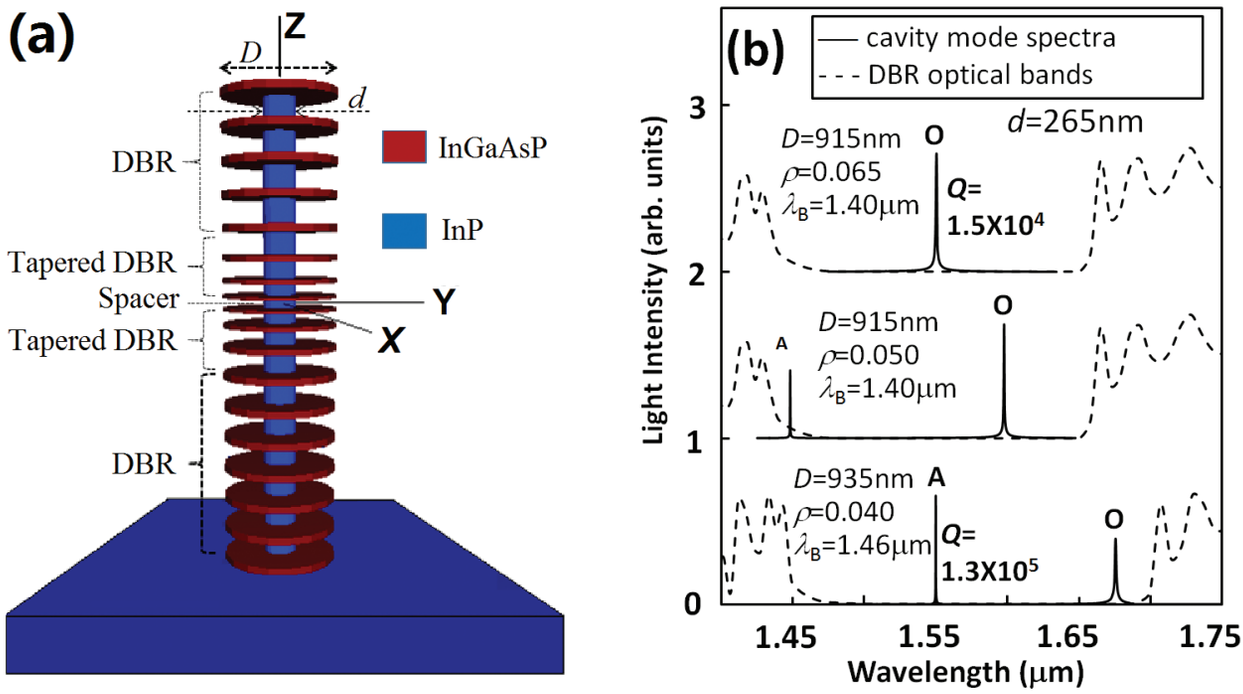

Figure 9. (a) Three-dimensional schematic demonstration of the InGaAsP/InP-air-aperture microcavity. (b) Examples of the calculated optical mode spectra with corresponding DBR optical bands. In (b), the lines for different design conditions are vertically shifted for clarity.

high-quality Si/SiO_2-InP hybrid pillar cavity [33] and the high-quality GaAs/AlGaAs monolithic pillar cavity [31]. By massively trying out different cavity geometrical parameters D, d, λ_B, and ρ, the optical properties were systematically studied. When d = 265 nm, D = 915 nm, λ_B = 1.40 μm, and ρ = 0.065, it is observed that the optical mode with the longest wavelength, i.e., the fundamental cavity mode, peaks at 1.550 μm with Q factor of 1.5 × 10^4, as shown by the topmost spectrum in **Figure 9(b)**. This is surprising because a similarly high InGaAsP/InP DBR pillar cavity exhibits Q factor of only a hundred or so. It indicates that the air apertures resolve the problem of low refractive index contrast in InP-based pillar cavities. We label this fundamental mode as mode O hereafter. It is roughly at the center of the DBR stopband, corresponding to an optimized condition. As shown by the middle spectrum in **Figure 9(b)**, when ρ is tuned to be 0.05, mode O shifts to a longer wavelength with Q factor decreasing to 6000. Meanwhile, there arises a new mode near the shorter stopband edge. Further changing ρ to be lower, the new mode, termed mode A hereafter, shifts toward the middle of stopband and its Q factor increases, while mode O is shifting toward the longer stopband edge with smaller and smaller Q factor. The lower spectrum in **Figure 9(b)** shows that, by changing all the three parameters D = 935 nm, ρ = 0.04, and λ_B = 1.46 μm, we obtain an optimized mode A, peaking at 1.550 μm and with Q factor of 1.3 × 10^5. This Q factor is one order of magnitude higher than the optimized mode O and even higher than that of a typical Si/SiO_2-InP hybrid pillar cavity with a similar pillar size [33]. At the same time, mode O becomes a peak near the longer stopband edge with Q factor below 3000.

It is worth stressing that the proposed cavity is a nanometer-scaled pillar structure since the cavity lateral size, especially the air-aperture diameter, is less than 1 μm. The direct result of this nanoscale is the small mode volume V, which is 1.08 and 0.94$(\lambda/n)^3$ for optimized modes O and A, respectively, where λ is the mode wavelength and n is the refractive index at the point of maximal light intensity. The light intensity distribution, which determines the mode volume through integrating over the cavity [1], is shown in **Figure 10**. We note that both modes are twofold degenerate with orthogonal main polarizations, but for simplicity, we arbitrarily select X as the main polarization direction to describe their properties. The colored patterns tell us that the light fields of both modes O and A are laterally well confined within the semiconductor cavity media, i.e., quite weak in the air, and vertically confined mainly within the tapered DBRs and the spacer region. This is resulted by the air apertures, which tend to compact the light fields laterally into an area with diameter d and vertically into a few DBR layers by increasing the reflective rate of DBRs.

The vertical distribution patterns in **Figure 10** also show the effect of adiabatic design in the tapered DBRs. That the light intensity extends over a few segments implies gentle confinement of light fields, which provides a reasonable explanation for the high Q factors [41] in both modes O and A. What is more important, there really exists a large difference in the two modes. Mode O has strong light fields both in the small-diameter InP spacer and the large-diameter InGaAsP layers, while mode A leaves its optical field mainly in the InGaAsP layers. With sub-wavelength lateral size $d < \lambda_B/n$, the InP spacer with air aperture is more subjective of leaking through the side wall. This is likely the reason why the optimized mode A has higher Q than mode O. In terms of the Z-dependent line profile of the main electric field along the X direction, E_X, mode O is symmetric, whereas mode A is antisymmetric to the cavity

http://dx.doi.org/10.5772/67499

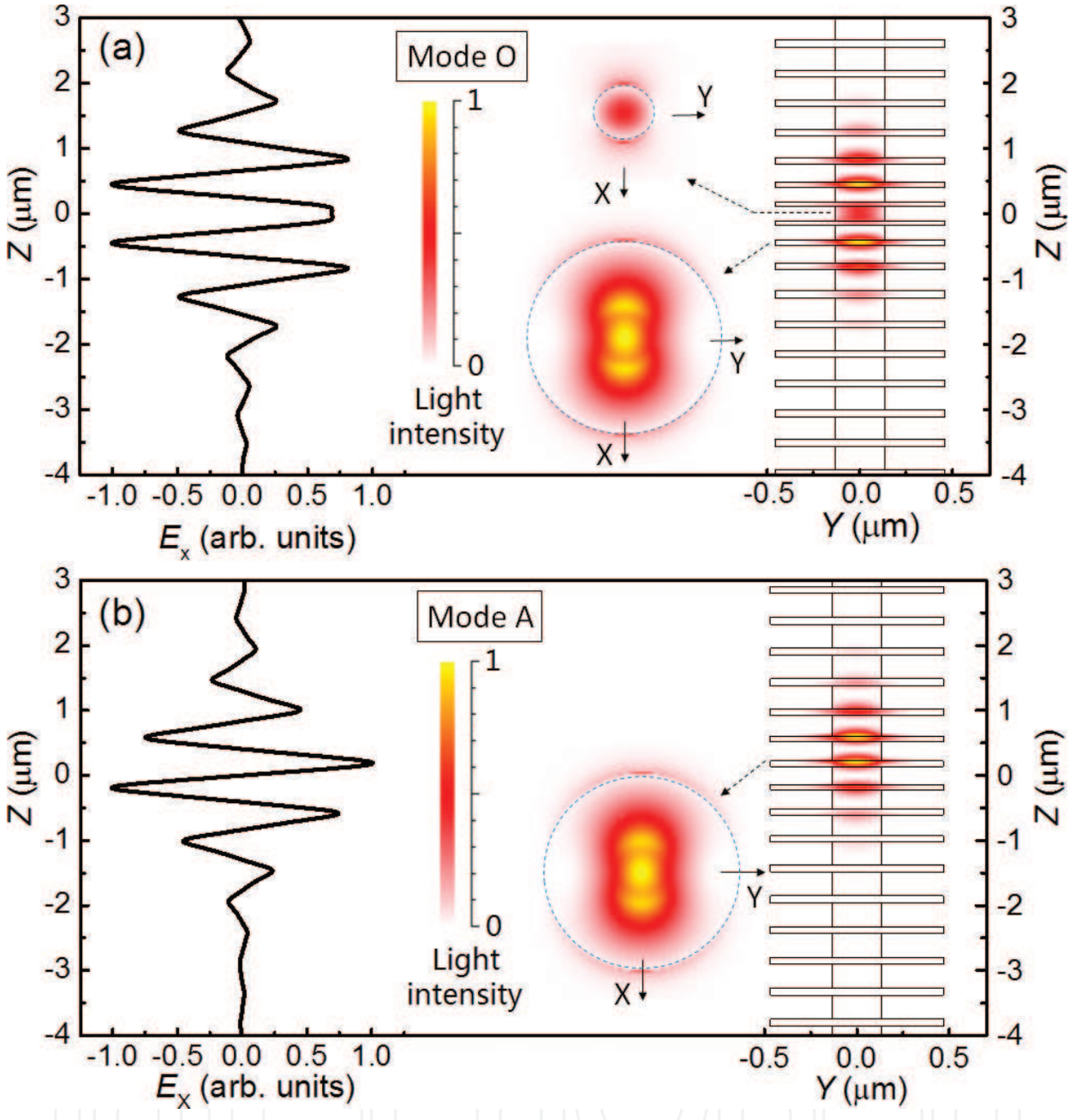

Figure 10. Line mode profiles along vertical Z direction and patterned mode profiles on the YZ and XY planes of the optimized optical (a) mode O and (b) mode A. Note that the line profiles are indicated by the x-polarized electric field, while the plane profiles are displayed by light intensity. The thin lines on the light intensity patterns show the outlines of the optimized cavities.

central plane $Z = 0$. This might be understood by a mode coupling between two fundamental modes corresponding to two differently sized nanopillars, as could bring in some new modes like bonding (symmetric) and antibonding (antisymmetric) states, since a present cavity looks like a mixture of two pillars with different sizes.

To use a cavity with optimized mode A, there seems a problem that the light source in the InP spacer has a weak interaction with the mode field due to minimum field intensity in the spacer.

As a matter of fact, 1.55 μm InAs QD can also be settled in the InGaAsP layer [42]. In addition, we find that exchanging InGaAsP and InP layers can give similarly good cavity properties.

Although we have obtained high Q factors on cavities with some special designs, it is necessary to further investigate the dependence on cavity design parameters, because the practical fabrication process may not be that exact. First let us look at the dependence on vertical size. For simplicity, we here characterize the effects of the tuning parameters λ_B and ρ in terms of the variation in spacer thickness $\Delta t_0 = t_0 - t_{0m}$, where t_{0m} is the optimized spacer thickness, since both of them give rise to changes in the spacer thickness t_0. As shown in **Figure 11(a)**, the mode wavelength λ varies linearly with the relative change in layer thickness at different rates. The tapering slope ρ has less effect on λ because it causes a more local geometric change in the cavity. Conservatively speaking, λ remains within 1.55 ± 0.05 μm range as the layer thickness changes within ±5%. To this degree of thickness deviation, the Q factors of modes O and A do not degrade a lot but remain over 1.3×10^4 and 10^5, respectively, although they would decay almost by factors of 3 and 10 with thickness deviation of ±15%. In more detail, λ_B degrades Q factor more weakly than ρ does because an entire geometric change by λ_B remains, to a high degree, the mode profile, while a local geometric change by ρ breaks the mode profile. By the way, mode O is more robust than mode A, since its Q factor remains over 10^4 with thickness change of ±10%. Given that t_0 is typically over 100 nm, ±5–10% precision means a layer thickness control error within ±5–10 nm, which is rather easy in modern epitaxial techniques enabling controllability at atomic layer level.

Now let us examine the dependence on lateral size. **Figure 11(b)** shows the variations in the cavity properties versus the relative change in cavity diameter $\Delta D/D_m = (D - D_m)/D_m$ and in air-aperture diameter $\Delta d/d_m = (d - d_m)/d_m$, where D_m and d_m are the optimized D and d values,

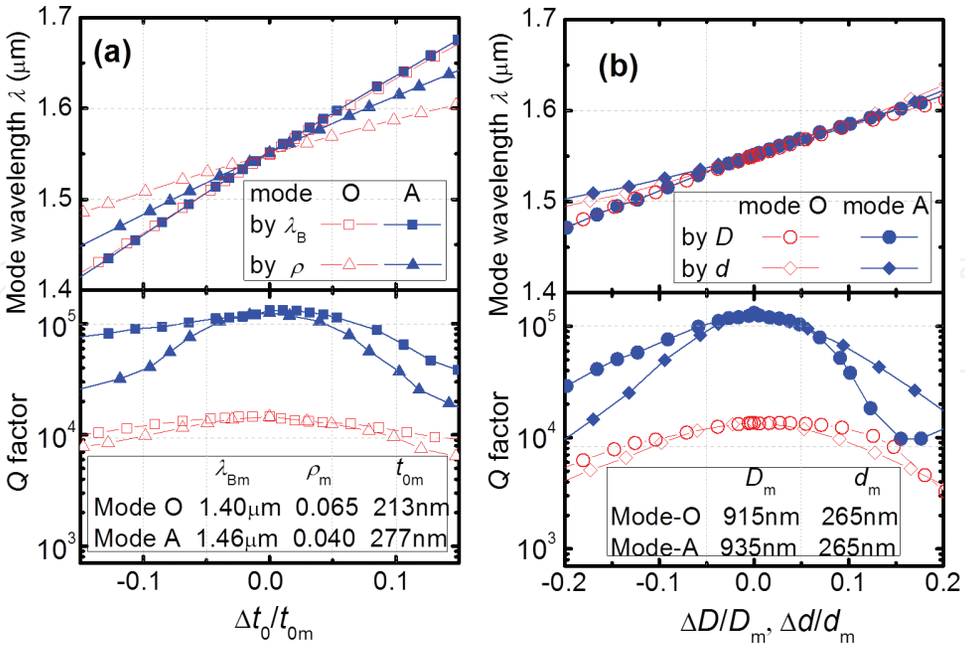

Figure 11. Varying mode wavelength λ and Q factor as the (a) vertical and (b) lateral sizes deviate from the optimized conditions for both modes O and A. Note that the vertical sizes, i.e., the layer thicknesses are tuned by λ_B or ρ but displayed in terms of the spacer thickness t_0. The lateral sizes are tuned by cavity diameter D or air-aperture diameter d.

respectively. It is normal that smaller lateral scale results in a shorter mode wavelength λ due to more localized geometrical confinement. A slight difference lies in the dependences of mode wavelength λ on D and d. The weakly sublinear change with D resembles conventional pillar cavities and can be explained by waveguide dispersion [26]. The super-linear dependence on d might be related to the existence of air apertures. Anyway, D and d have influences on λ to the similar extent in both modes O and A. It stays within 1.55 ± 0.05 μm as the lateral sizes deviate by up to ±10%. As to the Q factor, its degradation with D and d deviations, caused by deviated effective incident angle of light on the DBRs [18], is as much as that with thickness deviations. In a more quantitative view, ±5% change in D or d keeps mode O almost of no degradation and mode A over 10^5 in Q factor. Again, Mode O seems a little more robust than mode A, since ±8% deviation in lateral dimensions can keep its Q factor over 10^4. For a typical diameter of ~200 nm, the lateral size precision of ±5–10% means an error within ±10–20 nm. This degree of controllability has been already available in the state-of-the-art nanotechnology [43]. The robustness against the uncertainty of the fabrication process implies the high technical feasibility to fabricate high-quality microcavity at 1.55 μm telecommunication band.

Remember that in some cases, mode O and mode A coexist. Within the above tuning ranges, however, the main mode always stands with much higher Q factor than the other. There thus will be no serious interference from the useless mode when the main mode is working. By the way, Q versus D in mode A appears a little abnormal, i.e., Q rising back as D becomes large enough. It may result from coupling with higher-order optical modes as is mentioned in previous pillar cavities [25, 27].

With the simulated high quality, the proposed InGaAsP/InP-air-aperture micropillar cavity is hopefully a candidate for a 1.55 μm QD SPS. Let us analyze now how the application aspects of the proposed microcavity would be.

Above all, the likeliness of single-photon emission is enhanced by the nanoscale of the cavity. A single InAs/InP QD is a good single-photon emitter under usual excitation conditions [10, 11] since the excitation pulse duration can easily be in the order of picosecond or less, much shorter than the exciton lifetime of nanosecond order. Isolating a single QD is thus sufficient for single-photon emission. Supposing a high QD density of 6×10^{10} cm^{-2} and a good inhomogeneous width of ~50 meV, it is easy to get that there will be less than 1 QD resonant to a 1.55 μm cavity mode with Q factor of 10^4 (i.e., mode width less than 0.08 meV) in a pillar cavity with a diameter of 1 μm. This property highly guarantees the single-photon nature of an InAs/InP QD SPS composed of this micropillar cavity. In addition, the sub-micrometer-scaled structure is also beneficial to incorporating SPSs into a photonic integration chip, which is necessary in the future quantum information processing network. With Q/V over 3000, the Purcell factor F_p of a weak coupling cavity, simply speaking the enhancement degree of spontaneous emission of the light source, is estimated to be more than 100. This degree can reduce the spontaneous emission lifetime of InAs/InP QDs (a few ns [11]) to be shorter than the coherence time (~100 ps [16]). It suggests that a present cavity with optimized mode O ($Q \sim 10^4$ and $V \sim 1(\lambda/n)^3$) could be used as a photon-indistinguishable SPS [7] and GHz operating SPS at 1.55 μm band. In the case of strong coupling, which enables coherent transfer of quantum states between a light emitter and a cavity mode, theoretical criteria [37] suggest that $Q/V^{1/2} > 10^4$ is more than enough for a 1.55 μm InAs/InP QD

emitter. A present cavity with optimized mode A ($Q \sim 10^5$, $V < 1(\lambda/n)^3$) is thus able to realize coherently controllable single-photon devices at 1.55 μm band.

As compared to other pillar cavities, the microcavity proposed here takes some advantages. The widely used GaAs/AlGaAs DBR pillar cavity can also be of high-quality $Q > 10^5$ and sub-micrometer size [31]. If it is applied for 1.55 μm band, however, the pillar would be ~16 μm high, much more difficult to fabricate than the present ~7 μm high pillar. Furthermore, it is hard to contain 1.55 μm QDs in GaAs-based DBR structures. Therefore, a GaAs/AlGaAs pillar cavity is less usable as a 1.55 μm SPS than the present one. As to the InP-based materials, the calculations in Section 2 suggest that a conventional InGaAsP/InP DBR pillar cavity with a sub-micrometer diameter can work with Q factor of ~10^4 and Purcell factor of ~100 at 1.55 μm, able to weakly couple a single InAs/InP QD with a cavity mode. However, there should be ~40/70 periods of DBRs, meaning a pillar too high (~30 μm) to be currently producible. It is thus clear that, even only for weak coupling, InP-based DBR pillar cavity is much less suitable than the present one. The hybrid pillar cavities, such as Ta_2O_5/SiO_2–InP [22] or Si/SiO_2-InP [25, 33], are subject to interface defects and different thermal expansion coefficients. The present cavity consists of only InP-based epitaxial materials so that it is free of interface defects and thermal expansion difference. More significantly, it can be fabricated by a monolithic process, e.g., epitaxial growth for the multilayer structure, dry etching to form a pillar, and selective wet etching to develop air apertures. The fabrication process is obviously simpler and of lower cost than the techniques for fabricating hybrid pillar cavities [22].

There may arise a problem that the good cavity quality we have obtained may have a distance from that of a real cavity, because the above fabrication process could be not well determined to make an ideal cavity structure. One aspect may be that, with size less than 1 μm, process-induced surface roughness might degrade the cavity quality by, e.g., edge scattering [44]. At present, however, InP-based nanocavities, e.g., 100–400 nm-sized photonic crystal cavities, have readily exhibited practical Q factors above 10^4 [45] although surface roughness does exist. On the other hand, the present advanced techniques allow controlling sidewall surface roughness of InP-based nanostructures to be less than 1 nm while remaining of good optical quality [46, 47]. Primitive calculations on our nanocavities suggest that a sidewall roughness of 1 nm degrades the Q factor by 5–10%. There may be another aspect that the chemical etching influences the optical quality by introducing surface states [48]. Nevertheless, recent researches demonstrate that, when some suitable etchant and/or surface passivation are used, a wet-etched InP-based nanopillar presents nice optical properties [49]. A sophisticated wet-etching process would have only a minor effect on the quality of a nanocavity [50]. Furthermore, it is worth noting that InP/InGaAsP materials have a relatively low surface recombination velocity than GaAs/AlGaAs materials [51]. Consequently, a real cavity as here proposed could be expected to have optical quality very close to what is designed here.

We see that the InGaAsP/InP-air-aperture micropillar cavity proposed here is of high quality for weak and strong coupling, able to give single photons from InAs/InP QDs, producible by a monolithic process, robust against process uncertainty, and thus better than conventional GaAs/AlGaAs, InP/InGaAsP, and hybrid pillar cavities. It is therefore prospective as a candidate for 1.55 μm QD SPSs applied in silica-fiber-based quantum information system.

http://dx.doi.org/10.5772/67499

6. Summary

For quantum information processing over 1.55 μm silica-fiber-based networks, micropillar cavities containing QDs are designed to construct quantum devices such as SPSs. The straight way could be using micropillars composed of traditional InGaAsP/InP distributed Bragg reflectors (DBRs), which can in principle enable weak coupling between a single InAs/InP QD and an optical mode for an efficient 1.55 μm SPS. To reduce the difficulty in fabricating such ~30 μm high pillars, a pillar structure hybridizing semiconductor with dielectric materials is designed. Consisting of Si/SiO_2 DBRs and an InP active layer, such a micropillar cavity can greatly enhance the rate of single-photon emitting from an InAs/InP QD to be over GHz and thus serve as a photon-indistinguishable SPS. To further realize strong coupling between a 1.55 μm QD and an optical pillar mode, the Si/SiO_2-InP hybrid micropillar cavity is reformed by introducing tapered DBR structures into the central spacer. This new hybrid micropillar cavity can be diminished to have a sub-micrometer diameter, giving small mode volume and strongly ensuring single-photon emission. With Q factor as high as 10^5–10^6, this high-quality hybrid micropillar cavity can behave as a coherently controllable quantum device at 1.55 μm telecommunication band. To overcome the problems of complicated fabrication process and interface defects in the hybrid cavities, a novel structure, InGaAsP/InP-air-aperture micropillar, is finally proposed. This cavity can be fabricated by using a simple monolithic process. Owing to the air apertures and tapered distributed Bragg reflectors, such a microcavity with sub-micrometer diameter is capable of both weakly and strongly coupling a single quantum dot with an optical mode. It could thus be the promising candidate for a QD SPS at 1.55 μm telecommunication band applicable in silica-fiber-based quantum information processing.

Acknowledgements

This work was partially supported by the Project for Developing Innovation Systems of the Ministry of Education, Culture, Sports, Science and Technology (MEXT), Japan; by the Recruitment Program of Global Experts, China; and by the 1000 Talents Plan of Sichuan Province, China. We thank Dr. K. Takemoto, Dr. T. Miyazawa, Dr. M. Takatsu, and Prof. T. Yamamoto of Fujitsu Lab. Ltd., Japan, for their help in simulations and thank Prof. Zh. M. Wang of the University of Electronic Science and Technology of China for constructive discussions.

Author details

Hai-Zhi Song

Address all correspondence to: hzsong1296@163.com

1 Southwest Institute of Technical Physics, Chengdu, China

2 Institute of Fundamental and Frontier Sciences, University of Electronic Science and Technology, Chengdu, China

References

[1] Vahala KJ: Optical microcavities. Nature. 2003;424:839–846. DOI: 10.1038/nature01939

[2] Park SG, Kim SH, Kwon SH, Ju YG, Yang JK, Baek JH, Kim SB, Lee YH: Electrically driven single-cell photonic crystal laser. Science. 2004;305:1444–1447. DOI: 10.1126/science.1100968

[3] Shomroni I, Rosenblum S, Lovsky Y, Bechler O, Guendelman G, Dayan B: All-optical routing of single photons by a one-atom switch controlled by a single photon. Science. 2014;345:903–906. DOI: 10.1126/science.1254699

[4] Michler P, Kiraz A, Becher C, Schoenfeld WV, Petroff PM, Zhang L, Hu E, Imamoğlu A: A quantum dot single-photon turnstile device. Science. 2000;290:2282–2285. DOI: 10.1126/science.290.5500.2282

[5] Moreau E, Robert I, Gérard JM, Abram I, Manin L, Thierry-Mieg V: Single-mode solid-state single photon source based on isolated quantum dots in pillar microcavities. Appl. Phys. Lett. 2001;79:2865–2867. DOI: 10.1063/ 1.1415346

[6] Pelton M, Santori C, Vučković J, Zhang B, Solomon GS, Plant J, Yamamoto Y: Efficient source of single photons: a single quantum dot in a micropost microcavity. Phys. Rev. Lett.. 2002;89:233602. DOI: 10.1103/PhysRevLett. 89.233602

[7] Santori C, Fattal D, Vučković J, Solomon GS, Yamamoto Y: Indistinguishable photons from a single-photon device. Nature. 2002;419:594–597. DOI: 10.1038/nature01086

[8] Reithmaier JP, Sęk G, Löffler A, Hofmann C, Kuhn S, Reitzenstein S, Keldysh LV, Kulakovskii VD, Reinecke TL, Forchel A: Strong coupling in a single quantum dot–semiconductor microcavity system. Nature. 2004;432:197–200. DOI: 10.1038/nature02969

[9] Nomura M, Kumagai N, Iwamoto S, Ota Y, Arakawa Y: Laser oscillation in a strongly coupled single-quantum-dot–nanocavity system. Nat. Phys. 2010;6:279–283. DOI: 10.1038/NPHYS1518

[10] Takemoto K, Nambu Y, Miyazawa T, Sakuma Y, Yamamoto T, Yorozu S, Arakawa Y: Quantum key distribution over 120 km using ultrahigh purity single-photon source and superconducting single-photon detectors. Sci. Rep. 2015;5:14383. DOI: 10.1038/srep14383

[11] Takemoto K, Nambu Y, Miyazawa T, Wakui K, Hirose S, Usuki T, Takatsu M, Yokoyama N, Yoshino K, Tomita A, Yorozu S, Sakuma Y, Arakawa Y.: Transmission experiment of quantum keys over 50 km using high-performance quantum-dot single-photon source at 1.5 μm wavelength. Appl. Phys. Express. 2010;3:092802. DOI: 10.1143/APEX.3.092802

[12] Dixon AR, Yuan ZL, Dynes JF, Sharpe AW, Shields AJ: Continuous operation of high bit rate quantum key distribution. Appl. Phys. Lett. 2010;96:161102. DOI: 10.1063/1.3385293

[13] Sangouard N, Simon C, Minář J, Zbinden H, de Riedmatten H, Ginsin N: Long-distance entanglement distribution with single-photon sources. Phys. Rev. A. 2007;76:050301. DOI: 10.1103/PhysRevA.76.050301

[14] Gisin N, Pironio S, Sangouard N: Proposal for implementing device-independent quantum key distribution based on a heralded qubit amplifier. Phys. Rev. Lett. 2010;105:070501. DOI: 10.1103/PhysRevLett.105.070501

[15] O'Brien JL: Optical quantum computing. Science. 2007;318:1567–1570. DOI: 10.1126/science.1142892

[16] Kuroda T, Sakuma Y, Sakoda K, Takemoto K, Usuki T: Decoherence of single photons from an InAs/InP quantum dot emitting at a 1.3 μm wavelength. Phys. Stat. Sol. (c). 2009;6:944–947. DOI: 10.1002/pssc. 200880661

[17] Birowosuto MD, Sumikura H, Matsuo S, Taniyama H, van Veldhoven PJ, Nötzel R, Notomi M: Fast Purcell-enhanced single photon source in 1,550-nm telecom band from a resonant quantum dot-cavity coupling. Sci. Rep. 2012;2:321. DOI: 10.1038/srep00321

[18] Pelton M, Vučković J, Solomon GS, Scherer A, Yamamoto Y: Three-dimensionally confined modes in micropost microcavities: quality factors and Purcell factors. IEEE J. Quant. Electron. 2002;38:170–177. DOI: 10.1109/3.980269

[19] Faraon A, Fushman I, Englund D, Stoltz N, Petroff PM, Vučković J: Coherent generation of non-classical light on a chip via photon-induced tunnelling and blockade. Nature Phys. 2008;4:859–863. DOI: 10.1038/nphys1078

[20] Lin C-K, Bour DP, Zhu J, Perez WH, Leary MH, Tandon A, Corzine SW, Tan MRT: High temperature continuous-wave operation of 1.3- and 1.55-μm VCSELs with InP/air-gap DBRs. IEEE J. Sel. Topics Quantum Electron. 2003;9:1415–1421. DOI: 10.1109/JSTQE.2003.820924

[21] Gazzano O, Michaelis de Vasconcellos S, Arnold C, Nowak A, Galopin E, Sagnes I, Lanco L, Lemaître A, Senellart P: Bright solid-state sources of indistinguishable single photons. Nature Commun. 2013;4:1425. DOI: 10.1038/ncomms2434

[22] Dalacu D, Poitras D, Lefebvre J, Poole PJ, Aers GC, Willianms RL: InAs/InP quantum-dot pillar microcavities using SiO_2/Ta_2O_5 Bragg reflectors with emission around 1.55 μm. Appl. Phys. Lett. 2004;84:3235–3237. DOI: 10.1063/1.1728318

[23] Niklaus F, Stemme G, Lu JQ, Gutmann RJ: Adhesive wafer bonding. J. Appl. Phys. 2006;99:031101. DOI: 10.1063/1.2168512

[24] Jang SJ, Song YM, Yeo CI, Park CY, Lee YT: Highly tolerant a-Si distributed Bragg reflector fabricated by oblique angle deposition. Opt. Mater. Express. 2011;1:451–457. DOI: 10.1364/OME.1.000451

[25] Song HZ, Takemoto K, Miyazawa T, Takatsu M, Iwamoto S, Yamamoto T, Arakawa Y: Design of Si/SiO_2 micropillar cavities for Purcell-enhanced single photon emission at 1.55 μm from InAs/InP quantum dots. Opt. Lett. 2013;38:3241–3244. DOI: 10.1364/OL.38.003241

[26] Rivera T, Debray JP, Gérard JM, Legrand B, Manin-Ferlazzo L, Oudar JL: Appl. Phys. Lett. 1999;74:911–913. DOI: 10.1063/1.123407

[27] Gregersen N, Reitzenstein S, Kistner C, Strauss M, Schneider C, Höfling S, Worschech L, Forchel A, Nielsen TR, Mørk J, Gérard JM: Numerical and experimental study of the Q factor of high-Q micropillar cavities. IEEE J. Quantum Electron. 2010;46:1470–1483. DOI: 10.1109/JQE.2010.2052095

[28] Barnes WL, Björk G, Gérard JM, Jonsson P, Wasey JAE, Worthing PT, Zwiller V: Solid-state single photon sources: light collection strategies. Eur. Phys. J. D. 2002;18:197–210. DOI: 10.1140/epjd/e20020024

[29] Vučković J, Petlton M, Scherer A, Yamamoto Y: Optimization of three-dimensional micropost microcavities for cavity quantum electrodynamics. Phys. Rev. A. 2002;66:023808. DOI: 10.1103/PhysRevA.66.023808

[30] Kimble HJ: The quantum internet. Nature. 2008;453:1023–1039. DOI: 10.1038/nature07127

[31] Lermer M, Gregersen N, Dunzer F, Reitzenstein S, Höfling S, Mørk J, Worschech L, Kamp M, Forchel A: Bloch-wave engineering of quantum dot micropillars for cavity quantum electrodynamics experiments. Phys. Rev. Lett. 2012;108:057402. DOI: 10.1103/PhysRevLett.108.057402

[32] Zhang Y, Lončar M: Submicrometer diameter micropillar cavities with high quality factor and ultrasmall mode volume. Opt. Lett. 2009;34:902–904. DOI: 10.1364/OL.34.000902

[33] Song HZ, Takemoto K, Miyazawa T, Takatsu M, Iwamoto S, Ekawa M, Yamamoto T, Arakawa Y: High quality-factor Si/SiO_2-InP hybrid micropillar cavities with submicrometer diameter for 1.55-μm telecommunication band. Opt. Express. 2015;23:16264–16272. DOI: 10.1364/OE.23.016264

[34] Yariv A Optical Electronics. San Francisco: Saunders College; 1991.

[35] Lalanne P, Mias S, Hugonin J: Two physical mechanisms for boosting the quality factor to cavity volume ratio of photonic crystal microcavities. Opt. Express. 2004;12:458–467. DOI: 10.1364/OPEX. 12.000458

[36] Lalanne Ph, Hugonin JP, Gerard JM: Electromagnetic study of the quality factor of pillar microcavities in the small diameter limit. Appl. Phys. Lett.. 2004;84:4726–4728. DOI: 10.1063/1.1759375

[37] Auffèves A, Gerace D, Gérard JM, França Santos M, Andreani LC, Poizat JP: Controlling the dynamics of a coupled atom-cavity system by pure dephasing. Phy. Rev. B. 2010;81:245419. DOI: 10.1103/ PhysRevB.81.245419

[38] Bennett AJ, Patel RB, Shields AJ, Cooper K, Atkinson P, Nicoll CA, Ritchie DA: Indistinguishable photons from a diode. Appl. Phys. Lett. 2008;92:193503. DOI: 10.1063/1.2918841

[39] Kojima O, Nakatani H, Kita T, Wada O, Akahane K, Tsuchiya M: Photoluminescence characteristics of quantum dots with electronic states interconnected along growth direction. J. Appl. Phys. 2008;103: 113504. DOI: 10.1063/1.2936320

[40] Hillmer H, Daleiden J, Prott C, Römer F, Irmer S, Rangelov V, Tarraf A, Schüler S, Strassner M: Potential for micromachined actuation of ultra-wide continuously tunable optoelectronic devices. Appl. Phys. B. 2002;75:3–13. DOI: 10.1007/s00340-002-0957-x

[41] Zhou PY, Dou XM, Wu XF, Ding K, Luo S, Yang T, Zhu HJ, Jiang DS, Sun BQ: Photoluminescence studies on self-assembled 1.55-μm InAs/InGaAs/InP quantum dots under hydrostatic pressure. J. Appl. Phys. 2014;116:023510. DOI: 10.1063/1.4890013

[42] Akahane Y, Asano T, Song BS, Noda S: High-Q photonic nanocavity in a two-dimensional photonic crystal. Nature. 2003;425:944–947. DOI: 10.1038/nature02063

[43] Seo K, Wober M, Steinvurzel P, Schonbrun E, Dan Y, Ellenbogen T, Crozier KB: Multicolored vertical silicon nanowires. Nano Lett. 2011;11:1851–1856. DOI: 10.1021/nl200201b

[44] Shields AJ: Semiconductor quantum light sources. Nat. Photonics. 2007;1:215–223. DOI: 10.1038/ nphoton.2007.46

[45] Canet-Ferrer J, Prieto I, Muñoz-Matutano G, Martínez LJ, Muñoz-Camuniez LE, Llorens JM, Fuster D, Alén B, González Y, González L, Postigo PA, Martínez-Pastor JP: Excitation power dependence of the Purcell effect in photonic crystal microcavity lasers with quantum wires. Appl. Phys. Lett. 2013;102:201105. DOI: 10.1063/1.4807439

[46] Jiao Y, de Vries T, Unger R-S, Shen L, Ambrosius H, Radu C, Arens M, Smit M, van der Tol J: Vertical and smooth single-step reactive ion etching process for InP membrane waveguides. J. Electrochem. Soc. 2015;162:E90–E95. DOI: 10.1149/2.0371508jes

[47] Naureen S, Shahid N, Dev A, Anand S: Generation of substrate-free III–V nanodisks from user-defined multilayer nanopillar arrays for integration on Si. Nanotechnology. 2013;24:225301. DOI: 10.1088/0957-4484/24/22/225301

[48] Chang RR, Iyer R, Lile DL: Surface characterization of InP using photoluminescence. J. Appl. Phys. 1987;61:1995–2004. DOI: 10.1063/1.337995

[49] Oh DY, Kim S-H, Huang J, Scofield A, Huffaker D, Scherer A: Self-aligned active quantum nanostructures in photonic crystals via selective wet-chemical etching. Nanotechnology. 2013;24: 265201. DOI: 10.1088/0957-4484/24/26/265201

[50] Gehl M, Gibson R, Hendrickson J, Homyk A, Säynätjoki A, Alasaarela T, Karvonen L, Tervonen A, Honkanen S, Zandbergen S, Richards BC, Olitzky JD, Scherer A, Khitrova G, Gibbs HM, Kim JY, Lee YH: Effect of atomic layer deposition on the quality factor of silicon nanobeam cavities. J. Opt. Soc. Am. B. 2012;29:A55–A59. DOI: 10.1364/JOSAB.29.000A55

[51] Baba T: Photonic crystals and microdisk cavities based on GaInAsP–InP system. IEEE J. Sel. Top. Quantum Electron. 1997;3:808–830. DOI: 10.1109/2944.640635

IntechOpen